Asian Journal of Chemistry; Vol. 26, No. 21 (2014), 7087-7101

ASIAN JOURNAL OF CHEMISTRY

http://dx.doi.org/10.14233/ajchem.2014.17142

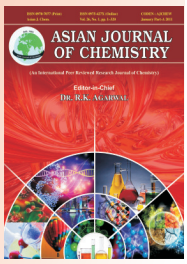

REVIEW

Preparation and Its Application of TiO_2/ZrO_2 and TiO_2/Fe Photocatalysts: A Perspective Study

KAMLU RAM GOTA and SUNDARAMURTHY SURESH*

Department of Chemical Engineering, Maulana Azad National Institute of Technology, Bhopal-462 051, India

*Corresponding author: E-mail: sureshpecchem@gmail.com

Received: 30 January 2014; *Accepted*: 28 February 2014; *Published online*: 30 September 2014; AJC-16078

The preparation and application of TiO_2/ZrO_2 and TiO_2/Fe photocatalysts were reviewed. We have prepared TiO_2/ZrO_2 and TiO_2/Fe photocatalyst by sol-gel process for degradation of phenolic compounds, decolourization of dye solution and removal of heavy metals in the wastewater. ZrO_2/TiO_2 composite photocatalytic was produced on the pure titanium substrate using *in situ* $Zr(OH)_4$ colloidal particle and the ZrO_2/TiO_2 composite shows a lamellar and porous structure which consists of anatase, rutile and ZrO_2 phases by the micro-arc oxidation technique. TiO_2 doped with Fe produced by the sol-gel method using titanium alkoxide as the precursor of titania as well as iron as dopant sources. Among synthesized photocatalysts, 0.1 M Zr and 0.15 M N supported on TiO_2 exhibited the best visible-light response and the highest NO photodegradation activity. The photocatalysts calcined at 500 °C are spherical particles with a crystallite size about 10-20 nm and the crystal phase presents a mixture of anatase (dominant phase) and rutile. The optimum doping amount of iron ions is 0.001 mol %. Although the addition of iron ions decreases the surface area of Fe/TiO_2, the photocatalytic activity of Fe/TiO_2 (*i.e.*, 0.001 mol %) is better than those of synthesized bare TiO_2 or P25. Consequently, the role of Fe may be responsible for the enhanced photodegradation, as compared to those from P25 or synthesized bare TiO_2.

Keywords: TiO_2, ZrO_2, Fe, Photocatalyst, Dye, Metals, Phenolic group.

INTRODUCTION

Water pollution is one of the main challenges problems and its affects humanity and animal's life health. Both organic and inorganic contaminants can be found in ground water wells and surface waters; these residues can cause adverse effects to the environment and to human health. Common water pollutants include: textile dye, petrochemical, pharmaceutical, distillery, tannery containing phenolic group; agro waste like insecticides, pesticides and herbicides[1-3]; inorganic compounds like heavy metals, such as mercury, arsenic, cadmium, silver, nickel, lead, noxious gases and pathogens like bacteria fungi and viruses[4,5].

4-Nitrophenol and its derivatives are used in the production of pesticides and as insecticides and herbicides[6,7]. Nitroaromatics are used in the production of explosives and 4-nitrophenol is used in the production of many synthetic dyes[8]. Therefore, 4-nitrophenol and its derivatives are common pollutants in many natural water and industrial wastewater. The UV/TiO_2 process, for instance, has been applied successfully to mineralize organic contaminants transforming them into inorganic species or converting them into organic species readily biodegradable[9,10]. Hence, the recent research is focused on the development of modified semiconductor photocatalysts to increase the efficiency of advanced oxidation processes[11-13]. Also, it is experimentally found that the presence of iron in Fe-TiO_2 catalysts enhances the photocatalytic activity of TiO_2 by acting both as hole and electron traps[14]. The contaminated water needs to be treated and re-used. The treatment of contaminated water is based on various mechanical, biological, physical and chemical processes[4]. After filtration and elimination of particles in suspension (primary treatments). Biological process results not sufficiently efficient since 4-nitrophenol is hardly removable due to its high stability and solubility in water. Physico-chemical processes have the main disadvantage that they are not destructive and they only transfer the contamination from one phase to another; hence, secondary wastes are produced and further treatments are necessary[15,16]. Biological treatment is ideal (secondary treatments). Unfortunately, there are certain products, called bio-recalcitrant (non-biodegradable), for which much more effective nonreactive systems, such as air stripping, adsorption on granulated activated carbon, incineration, ozone and oxidation (tertiary treatments), are needed. These processes aim to treat wastewaters and therefore improve water quality, but some of these technologies such as adsorption and filtration merely concentrate the pollutants by transferring them to other phases. Therefore, management of toxic chemicals with strict environmental

legislation drives the development of clean and green processes, to eliminate the pollutants before they are disposed into the environment.

Advanced oxidation processes for bio-recalcitrant wastewater treatment is universally recognized today and many researchers around the world are devoting their efforts to the development of these processes[17,10]. Although they make use of different reaction systems, advanced oxidation processes are all characterized by the same chemical feature: the production of hydroxyl radicals ($OH^{\bullet}$). A useful attribute of the hydroxyl radicals is their very low selectivity. These radicals can virtually destroy any organic contaminant present in water. They can even destroy pollutants that are not amenable to biological treatments, which are all characterized by high chemical stability and difficulty to be completely mineralized[18,10]. In order to apply a decontamination technique to these cases, it is necessary to adopt reactive systems much more effective than those adopted in conventional purification processes. Among advanced oxidation processes, heterogeneous photocatalysis has confirmed its efficiency in degrading a wide range of organic contaminants into CO_2, water and some readily biodegradable mineral acid[4]. Moreover, photocatalysis is not restricted to water purification only, as it is also used in air purification, self cleaning surfaces, among others[19]. Photocatalysis processes make use of solid semiconductors that are activated with UV light.

The most common photocatalyst is the TiO_2. So far, the application of the TiO_2 mediated photoreactions for water treatment is still experiencing a series of technical challenges *e.g.*, (i) separation of TiO_2 catalyst after water treatment is considered the major obstacle (ii) catalyst development with a strong absorption in the visible spectrum region (iii) understanding the theory behind common reactor operation parameters, such as light intensity distribution inside photocatalytic reactors and (iv) addressing mathematical inconsistencies commonly found in the kinetic modeling. Moreover its activity is still not high enough to be suitable for commercial application. In order to enhance the activity of catalyst, many efforts have been paid to modify TiO_2 by adding some transition metals, such as Fe^{3+}, Mo^{6+}, La^{6+}, Gd^{3+}, W^{+} in the past two decades. It has been found that addition of ZrO_2 could enhance the activity significantly and another way to enhance the photocatalytic activity is the coating of other materials, including metal ions and semiconductors, onto the surface of TiO_2 nanoparticles. The coupling of two semiconductors provides a novel approach to achieve a more efficient charge separation, an increased lifetime of the charge carriers and an enhanced interfacial charge transfer to adsorbed substrates. Different methods for the preparation are thermal chemical vapor deposition, hydrolysis deposition, spray pyrolysis, radiofrequency magnetron sputtering, sol-gel method and so on. Among these methods, sol-gel process has notable advantages such as high purity, good uniformity of the film microstructure, low temperature synthesis, easily controlled reaction condition. This review includes the coupling of heterogeneous metals like titania and zirconia, as well as titania and ferric oxide semiconductors in order to increase the catalytic activity.

Micro-arc oxidation is a processing technique which can convert the surfaces of valve metals, such as aluminum, magnesium and titanium, into ceramic coatings[20-22]. The technique is considered to be appropriate for immobilizing the TiO_2 photocatalyst, because the distinct properties of TiO_2 formed *via* micro-arc oxidation include chemical durability, large specific surface area, remarkable thickness and good adhesion to metal substrate. There are only few reports on growing composite TiO_2 photocatalytic material by micro-arc oxidation method. Some semiconductors have been used to couple with TiO_2 in order to improve its photocatalytic activity. Among these semiconductors, ZrO_2 is considered an appropriate semiconductor coupled with TiO_2 because it is beneficial for the increase of surface area, the stabilization of anatase and the existence of stable electron-hole pairs[23-25]. As far as we know, ZrO2/TiO_2 composite photocatalytic material has not been prepared by micro-arc oxidation technique to date. Luo *et al.*[26] prepared ZrO_2/TiO_2 composite photocatalytic using *in situ* $Zr(OH)_4$ colloidal particle by micro-arc oxidation technique.

Compared to pure TiO_2, TiO_2-ZrO_2 composites have tunable composition, abundant phases and more attractive photocatalysis properties. Numerous efforts have been devoted to synthesize TiO_2-ZrO_2 with different morphologies[27-29]. It is postulated that ordered TiO_2-ZrO_2 composites with wide Ti/Zr ratios will possess specific photocatalytic properties due to the large surface area, unsaturated titanium (IV) sites, oxygen vacancies existing on the surface and high thermal stability. As for synthesis, as mentioned above, ordered mesoporous TiO_2 with crystalline walls are easily achieved. However, ordered mesostructured TiO_2-ZrO_2 has been rarely reported. Caruso *et al*. reported porous titania/zirconia with pore of 1 Lm using polymer gel template[30] and proved these materials had good photocatalytic activities for decomposition of organic molecules. Liu *et al.*[31] obtained mesoporous TiO_2-ZrO_2 composites utilizing triblock copolymer as template. Zhou *et al.*[32] showed disordered mesostructures. To the best of our knowledge, highly ordered mesoporous multi-metal composites such as TiO_2-ZrO_2 composites with varied Ti/Zr ratios have not been reported. Although some specific conclusions have been drawn from above studies on photocatalytic properties of TiO_2 with ordered mesoporous structures, there is a lack of systematic synthesis and detailed measurements of photocatalytic properties of ordered mesoporous TiO_2-ZrO_2 composites.

Compared with pure TiO_2, the Fe-doped TiO_2 has higher specific surface area, low combination of electrons and holes and red-shift in light absorption[33-36]. Most dopants were papered by sol-gel method, although some of them combined with many other methods, morphology of sample is irregular. However, it is easy to dope all kinds of elements if needed, especially some lightly dope. One can precisely control the chemical composition of the material by sol-gel method[37-39]. The dopants synthesized by anodic oxidation method can obtain highly ordered nanotubes, but the content of elements doped into TiO_2 was very poor. Fe-doped TiO_2 is mainly applied in photocatalytic degradation or served as anode of dye-sensitized solar cells or as pigments and as disinfection and sterilization with UV. With the development of technology and increasing in demand for work, the TiO_2 with special properties play an important role in many fields. Someone has been trying applying TiO_2 with special properties in (as) sensing material, light cracking water into hydrogen, lithium ion battery, super-

hydrophilic/superhydrophobic conversion film[40], field emission device materials and so on[41]. The development of TiO_2 would be a new industry, because it can be synthesized in many ways and appeared on many kinds of morphology, besides described in this essay, such as can be noticed that the effect of iron species content in Fe-TiO_2[42].

Titanium dioxide represents an effective photocatalyst for water and air purification and for self-cleaning surfaces. Additionally, it can be used as an antibacterial agent because of strong oxidation activity and superhydrophilicity[43]. Titanium dioxide shows relatively high reactivity and chemical stability under ultraviolet light ($\lambda < 387$ nm), whose energy exceeds the band gap of 3.3 eV in the anatase crystalline phase. The development of photocatalysts exhibiting high reactivity under visible light ($\lambda > 400$ nm) should allow the main part of the solar spectrum to be used, even under poor illumination of interior lighting. Several approaches to modifying TiO_2 have been proposed: metal-ion implanted TiO_2 (using transition metals: Cu, Co, Ni, Cr, Mn, Mo, Nb, V, Fe, Ru, Au, Ag, Pt)[44-46] reduced TiOx photocatalysts[47], non-metal doped-TiO_2 (N, S, C, B, P, I, F)[48-50] composites of TiO_2 with semiconductor having lower band gap energy (*e.g.*, Cd-S particles[51], sensitizing of TiO_2 with dyes (*e.g.*, thionine)[52] and TiO_2 doped with upconversion luminescence agent[53,54]. The aim of this study is to review TiO_2 doped with iron. The effect of the doping process on the fundamental physicochemical properties for all obtained samples was evaluated. We have prepared TiO_2/ZrO_2 and TiO_2/Fe photocatalyst by sol-gel process. Various parameters and applications over prepared photocatalyst and validated with literature report. Literature study of TiO_2/ZrO_2 and TiO_2/Fe for degradation of phenolic compounds, decolourization of dye solution and removal of heavy metals also discussed.

Synthesis of TiO_2-ZrO_2 /TiO_2-Fe photocatalyst by sol-gel method

TiO_2-ZrO_2 composite: All the chemicals used were analytically pure. The TiO_2/ZrO_2 photocatalytic materials were synthesized with a sol-gel method. For the preparation of catalyst, titanium isopropoxide and zirconium oxychloride octahydrate were used as the starting materials. Desired quantity of titanium isopropoxide and anhydrous ethanol were premixed for 45 min by stirring with a magnetic stirrer. 12 wt. % of zirconium oxychloride octahydrate was dissolved in distilled water to form a solution. Under vigorous stirring, the solution is added dropwise into the previous mixture. Appropriate amount of HCl (dil.) was added to adjust pH of the solution to around 2. The temperature of the reaction system was maintained at room temperature for slow hydrolysis. After 14 h, initial solution transformed to an opaque sol and sol obtained was used as precursor sol. The resultant sample was taken out and washed several times by double distilled water and absolute ethanol to remove excessive organic or inorganic impurities and then dried at 120 ºC. At last, the composite powders are calcined at 500 ºC in a furnace for 3 h. Quantitative as well as qualitative composition analysis of prepared alumina was determined by EDS spectrum obtained from SEM. The compositional analysis of titania-zirconia composite catalyst calcined at 500 ºC at 3 h was found. The chemical composition of TiO_2-ZrO_2 photocatalyst (wt. %) was 4.32 Zr, 48.12 Ti and oxygen 46.75, respectively (Fig. 1).

It can be confirmed from XRD patterns that TiO_2 in prepared samples was identified as an anatase phase. The degree of crystallinity depends on the amount of Zr. The XRD of catalysts have significant diffraction peaks representing the characteristics of the anatase phase of TiO_2 and various TiO_2 composite catalysts. The XRD analysis indicates that as the ZrO_2 component increases, it prevents the phase transformations from anatase to rutile, which is favorable to the photocatalytic reaction since the anatase phase is known to have much higher activity than the rutile phase. The scanning electron micrographs (SEM) of the TiO_2/ZrO_2 composites are studied. The SEM images of all three composites display similar morphology. From the images it is clear that the catalyst particles are spherical in shape. Thus SEM images are clear evidence for complete homogeneity of Zr^{4+} with TiO_2. Single highly homogeneous aggregates are significant for photo catalysis as they can absorb even bulky pollutants. BET surface areas of titania-zirconia composites depend on the quantity of zirconia. The largest surface area (171 m^2/g) and pore volume (0.63 mL/g) were observed. The high surface and pore volume of prepared TiO_2/ZrO_2 is due to porous nature of the oxides formed through the sol-gel method. A slight decrease in the high surface area and pore volume after addition of high amount of zirconia has been noted which occurs due to various factors such as penetration of the deposited active oxides into the pores of the support thereby narrowing its pore volume, blocking of some of the micro pores and solid state reaction between the dispersed active oxide and the supporting oxide.

Fig.1. Photoview of prepared TiO_2-ZrO_2 composite

TiO_2-Fe doped photocatalyst: For preparation of high active nano-sized TiO_2/Fe_2O_3 composite photocatalytic materials by sol-gel method was followed. According our choice, the weight of TiO_2 and Fe_2O_3 were taken for different ratios. Here, TiO_2 and FeO_3 have been used. The certain amount of TiO_2 and Fe_2O_3 were taken and TiO_2 was dissolved in ethanol and same Fe_2O_3 was mixed by double distilled water for 2 h. After 2 h under vigorous stirring, the solution is added dropwise into the previous mixture. So that the mixing should be uniformly. After 14 h, the initial solution transformed to an opaque sol and the sol obtained was used as precursor sol. The resultant sample was taken out and washed several times by distilled water and absolute ethanol to remove excessive organic impurities and then dried at 120 ºC. At last, the composite powders are calcined at 500 ºC in a furnace for 3 h. A series of samples with different mass ratio of Fe/Ti are

prepared with different Fe content such as 0, 10 and 20 wt. % and these were denoted by FT-1, FT-2 and FT-3, respectively (shown in Fig. 2).

Fig. 2. Photoview of prepared TiO_2-Fe catalyst

Synthesis of TiO_2-ZrO_2 composite: Mesostructured ZrO_2-TiO_2 nanoparticles with different ZrO_2 contents have been synthesized by an ionic liquid [1-hexadecane-3-methyl-imidazolium bromide, (16 MIM + Br)] assisted hydrothermal route[55]. The obtained ZrO_2-TiO_2 materials exhibit large specific surface area (193.8 m^2/g) and uniform pore size (about 6.8 nm). Introduction of ZrO_2 species can effectively suppress phase transformation from anatase to rutile and promote thermal stability of ZrO_2-TiO_2 materials. The photocatalytic activity of the ZrO_2 -TiO_2 sample is higher than that of the TiO_2 sample and commercially available Degussa P25[55]. The high photocatalytic activity can be attributed to stronger adsorption in the ultraviolet region, higher specific area, smaller crystal size and increased surface OH groups. During photocatalytic degradation of *p*-chlorophenol -TiO_2 under UV irradiation, the ZrO_2-TiO_2 samples reveal high activity compared with pure TiO_2 and commercially available Degussa P25.

The typical synthesis process was described by Liu *et al.*[55] as following: 0.005 mol of C16 MIMBr was dissolved in 15 mL of distilled water with vigorous stirring at 40 °C for 0.5 h. Then certain amount of tetrabutyl orthotitanate and $Zr(NO_2)_4{\cdot}5H_2O$ (total amount of Ti plus Zr is 0.015 mol) were added into the above solution. The molar ratios of Zr in the composition were set for 4, 10, 20 and 30 %, which were denoted as ZT4, ZT10, ZT20 and ZT30, respectively. After stirring for 0.5 h, pH value was adjusted to 9-10 by dropwise addition of ammonia solution. After stirring for another 2 h, the homogeneous sol was transferred to a 100 ml Teflon-lined stainless steel autoclave at 100 °C for 2 days. Then the product was recovered by filtration, washed thoroughly with deionized water and dried at 100 °C over night. The as-synthesized material was calcined in air at 400 °C for 4 h to remove the template. For comparison, pure TiO_2 was prepared using the same method without the addition of $Zr(NO_2)_4{\cdot}5H_2O$.

Yuan *et al.*[56] synthesized mesoporous TiO_2-ZrO_2 by following procedure: 0.7-1.0 g Pluronic F127 or 0.5-1.0 g Pluronic P123 was dissolved in 10 mL of ethanol at room temperature. Then quantitative $[CH_3(CH_2)_3O]_4$ Ti and $ZrOCl_2{\cdot}8H_2O$ were added (total amount of Ti plus Zr is 5 mmol) into the above solution with vigorous stirring. The composition of Ti/Zr/F127/EtOH (molar ratio) was varied in the range of (0.5-4.5)/(4.5-0.5)/(0.05-0.08)/170. The mixture was covered with polyethylene film. After stirring for at least 2 h at room temperature, the homogeneous sol was transferred to an oven and underwent solvent evaporation. After two days of aging under desired temperature and humidity [temperature: 40 °C, relative humidity (RH): 50 %], the gel product was dried in another oven at 100 °C C for 1 day. Calcinations was carried out by slowly increasing temperature from room temperature to 400 °C (1 °C/min ramping rate) and heating at 400 °C for 4 h in air. High temperature treatment was carried out in air for 1 h with a temperature ramp of 10 °C/min.

The XRD patterns demonstrate that all the samples are present in well-crystallized anatase[55]. No significant shifts of the principal diffraction peaks are observed, indicating that ZrO_2 is present in a separate phase rather than incorporated into the TiO_2 lattice. The ZrO_2 species are highly distributed in the TiO_2 structure and thus, no significant diffractional peaks indicative of ZrO_2 phase can be observed even for the 30 % ZrO_2-TiO_2 sample. However, with increase of zirconium content, the peak of anatase becomes weaker and wider gradually, indicating that the crystallinity of TiO_2 anatase deteriorates and the crystallite size decreases. It can be seen that with ZrO_2 doping, the particle size of TiO_2 became smaller, suggesting that the presence of ZrO_2 can suppress the anatase crystallite growth.

ZrO_2 consists of mainly the cubic phase with very small amount of tetragonal phase as seen from XRD patterns[57]. TiO_2 exists as anatase phase and contains very little rutile phase. XRD pattern of CdS shows sharp narrow peaks indicating that it is a highly crystalline material and it exists as hexagonal wurtzite phase. XRD pattern of ZTC composite shows clearly the peaks corresponding to anatase TiO_2, cubic ZrO_2 and hexagonal CdS indicating that it is a mixture of these phases. TEM image of pure CdS indicates that its particle size is higher than that of ZTC composite and exists in an aggregated form. SAED pattern of CdS consists of spotty rings suggesting that it is a polycrystalline material. The EDX analysis results indicate that the amount of TiO_2 and CdS on ZrO_2 is 27 and 25% (by wt.), respectively, which is close to the starting composition. The BET surface areas of TiO_2, CdS, ZrO_2, TC, ZC and ZTC are 42, 20, 48, 33, 35 and 38 m^2/g, respectively. The surface areas of the composite samples are comparable and more than that of pure CdS. The XRD patterns of films prepared in different electrolytes are shown by Luo *et al.*[26]. The characteristic peaks of Ti are detected from pure titanium substrates. A mixed phase of anatase, rutile and ZrO_2 occurs in the ZrO_2/TiO_2 composite. The surface micrographs of prepared photocatalyst in different electrolytes was analysed by SEM, the surface of ZrO_2/TiO_2 composite exhibits a lamellar and porous micro-structure. Furthermore, on the surface of composite, there are many bright particles which are agglomerated. The EDX analysis of the bright particle mainly contain 22.95 % Zr, 11.13 % Ti and 65.91 % O (mole fraction), which is similar to the chemical compositions of the mixture of ZrO_2 and TiO_2. The surface of pure TiO_2 also exhibits a porous microstructure, the surface of pure TiO_2 is relatively smooth compared with the ZrO_2/TiO_2 composite. Mild spark discharge means fewer discharge channels on the surface of pure TiO_2 compared with the ZrO_2/TiO_2 composite, which results that the surface of pure TiO_2 is relatively smooth compared with the ZrO_2/TiO_2 composite.

The thicknesses of the ZrO_2/TiO_2 composite and the pure TiO_2 are approximately 10 and 3 μm, respectively. Furthermore, compared with the pure TiO_2, there are many micropores in the inner layer of the ZrO_2/TiO_2 composite. The growth of the micro-arc oxidation is the result of melting and solidifying of oxide through the discharge channels, therefore, more discharge channels mean faster growth rate and the ZrO_2/TiO_2 composite should be thicker than the pure TiO_2 during the same period. The differences of the surface and cross-section morphologies between the two materials are attributed to more violent spark discharge during the micro-arc oxidation process of ZrO_2/TiO_2 composite. For ZrO_2/TiO_2 composite, the lamellar and porous microstructure, agglomerated ZrO_2/TiO_2 mixed particles and micro-pores in the inner layer of composite should be responsible for providing more surface sites, in which more organic compounds and photons can be absorbed compared with the pure TiO_2.

Physicochemical properties of the mesoporous ZrO_2-TiO_2 composites prepared with different Ti/Zr ratios and calcination temperature were analyzed through various techniques[58]. The highest surface area (250 m^2/g), pore size (3.5 nm) and pore volume (0.29 cm^3/g) were found to be at 400 °C in the meso-10TZ sample. Characterization of the composite Powder XRD patterns of the composite sample and the constituent compounds are shown by Yang *et al.*[57]. ZrO_2 consists of mainly the cubic phase with small amount of tetragonal phase as seen from the asymmetry of the peak around 29, 34, 49 and 59°. TiO_2 exists as anatase phase and contains little rutile phase. XRD pattern of CdS shows sharp narrow peaks indicating that it is a highly crystalline material and exists as hexagonal Wurtzite phase. XRD pattern of ZTC composite shows clearly the peaks corresponding to anatase TiO_2, cubic ZrO_2 and hexagonal CdS indicating that it is a mixture of these phases. TEM image of pure CdS indicates that its particle size is higher than that of ZTC composite and exists in an aggregated form. SAED pattern of CdS consists of spotty rings suggesting that it is a polycrystalline material.

Nitrogen doped ZrO_2/TiO_2 photocatalysts were synthesized *via* a sol-gel method[59]. First, 0.1 M titanium tetraisopropoxide was incorporated with 100 mL of isopropyl alcohol by vigorous stirring for 1 h. Then, $ZrO(NO_3)_2$ and hexadecyl termethylammonium bromide were mixed together with a molar ratio, Zr/(Zr + Ti), of 0.5 and vigorously stirred for 0.5 h. Polyethylene glycol (2 g) was dissolved in isopropyl alcohol, added to the hexadecyl termethylammonium bromide solution and stirred again for 0.5 h. The two kinds of solutions were mixed and stirred until a homogenous mixture was obtained. Here, the concentration of hexadecyl termethylammonium bromide was changed from 0.1 to 0.2 M for controlling the level of nitrogen doping. The prepared solution was calcined for 2 h in an electric furnace at 500 °C in air at a heating rate of 5 °C /min TiO_2 without ZrO and hexadecyl termethylammonium bromide was also prepared to compare photocatalytic activity with the nitrogen doped ZrO_2/TiO_2 photocatalyst.

Synthesis of Fe-TiO_2 photocatalyst: TiO_2 (anatase phase, specific surface area 8 m^2/g) was dried, crushed and sieved to obtain particles with a diameter smaller than 0.1 mm[60]. Loading was performed by impregnating TiO_2 with aqueous solutions of $Fe(NO_3)_3 \cdot 9H_2O$ by an incipient wetness impregnation method as described. The mixture [TiO_2 and $Fe(NO_3)_3$] was stirred at room temperature during 24 h. Subsequently the catalysts were dried overnight at 393 K by using an oil bath. Finally, the catalysts were calcined for 5 h in a furnace whose temperature was increased from room temperature to 350 °C. After calcinations, the catalysts (1, 3, 5 and 8 %) Fe-TiO_2 was stored in a desiccator.

The doped-TiO_2 materials were prepared following two different methods. **The first method:** Solution A was prepared by adding 0.049 mol of titanium tetraisopropoxide to 1.304 mol of 2-propanol. A certain amount of $Fe(NO_3)_3$ was dissolved in 0.782 mol of 2-propanol (solution B). Subsequently, solution B and ammonia (catalyst-solution C) were introduced to solution A, at a constant rate of 5 and 1 cm^3/min, respectively. The resulting solution was vigorously stirred. When dosing of solutions B and C was terminated, the emulsion obtained was mixed for 0.5 h. **Second method:** Solution A was prepared by adding 15 mL 0.049 mol of titanium tetraisopropoxide to 0.670 mol of 2-propanol. At first, a certain amount of $Fe(NO_3)_3$ was dissolved in 100 mL 0.782 mol of 2-propanol and then the solution obtained (solution B) was dosed to solution A at a constant rate of 5 cm^3/min. The obtained solution was vigorously stirred. Next 0.033 mol of ammonia was dissolved in 0.670 moles of 2-propanol (solution C) and then the resulting mixture was introduced to a mixture of solution A and B, at a constant rate of 1 cm^3/min. When dosing of solution C was terminated, the obtained emulsion was mixed for 0.5 h. The concentrations of Fe calculated for mass of the dry sample of titania were 0.10; 0.25; 0.57; 0.75; 1.00; 1.70 and 2.80 % mass, respectively. Classification of the obtained products was realised in analogous way as in the case of preparation titanium dioxide. The final products of Fe-doped titania has a yellow colour.

Titanium(IV) isopropoxide(TTIP) and ferric chloride ($FeCl_3$) were used as starting materials and ethanol was used as solvent. The TiO_2 doped Fe^{3+} (0.3, 0.5, 0.8. and 1.0 mol %) powders were prepared through a conventional sol-gel method. Firstly, titanium(IV) isopropoxide was dissolved in ethanol, mixed with $FeCl_3$ by stirring for 15 min at room temperature and followed by adding droplets of 4 M NH_3 into the solution until pH about 3-4[61]. Finally, distilled water was slowly added to the solution by stirring for 0.5 h. The solution was dried at 105 °C for 24 h and calcined at the temperature 400 °C for 2 h. The synthesized powder was ground and submitted to determine the particle size by a light scattering particle analyzer before using as a photocatalyst.

The TiO_2 samples were synthesized using hydrothermal method. $TiCl_4$ and $Fe(NO_3)_3$ were used as the precursors of TiO_2 and Fe ions. 4 mL $TiCl_4$ was added to 400 mL ice distilled water under vigorous stirring and then, the resulted solution was stirred for 24 h at room temperature. Subsequently, aqueous solution of ammonia (1: 9) was added to adjust the solution pH to 7 to get $Ti(OH)_4$ precipitation[62]. The precipitation was filtered and cleaned using distilled water for many times. Afterwards, the $Ti(OH)_4$ precipitation was dispersed in ice-distilled water. 30 % H_2O_2 was dropped until it became yellow and transparent. A designed amounts of $Fe(NO_3)_3$ were

added under stirring and then, the solutions were heated in enclosed autoclave for 12 h at 160 °C to get Fe-doped TiO_2 sols. A series of Fe-doped TiO_2 samples were prepared with the Fe: Ti molar ratio being 0, 0.1, 0.3, 0.5, 0.8, 1, 2 and 5 at. %, respectively. Finally, the hydrosols were dried at 40 °C to obtain the powders.

The XRD patterns of Fe-doped TiO_2 samples almost coincide with that of the bare TiO_2 sample. It can be noticed that the presence of anatase TiO_2 type structure in all Fe loaded TiO_2 catalysts, without significant difference with the bare TiO_2 This finding can be explained by considering that the Fe content in the Fe-TiO_2 samples is below the detection limit or that amorphous iron oxides species are very dispersed onto the surface of TiO_2 particles. Analysis of SEM picture shows that 1 % Fe-doped TiO_2 catalyst contains a higher number of irregular shaped particles. Moreover, the sizes of the Fe-doped particles, consisting of aggregates of tiny crystals, are smaller compared to that of the bare TiO_2 sample, in agreement with the XRD results[60].

The titanium dioxide is characterized by a monomodal particle size distribution with a relatively wide band covering the diameter range of 955-2670 nm[63]. The maximum volume contribution of 28.4 % corresponds to agglomerates of 1720 nm in diameter. The polydispersity index of TiO_2 is 0.153, which means that this sample is rather homogeneous. The SEM microphotograph of the titanium dioxide studied confirms the presence of particles of micro-sized diameter (corresponding to those indicated in the particle size distribution), their almost spherical shape and high homogeneity. The fundamental parameters determining the surface activity of the doped samples, the surface area (BET) and pore size distribution were considerable decrease in the surface area relative to that of the pure sample was observed for all doped samples. Addition of any of dopants also resulted in a decrease in the pore diameters relative to those of native TiO_2, irrespective of the quantity of dopant. Decrease of the BET surface areas was observed together with increasing Fe amount in the sample structure. The surface composition of the obtained samples was studied by the EDS technique. From the elemental mapping mode, highly and uniformly dispersed Fe on the TiO_2 support was observed[63]. This implies good interaction between dopant and support in the preparation process using the sol-gel method. The EDS technique was used to detect the amount of Fe in the titania structure. Doped titania samples contain -0.12 and -0.56 % mass of Fe were produced *via* first method using 0.10 and 0.57 % mass of Fe as a dopant. It can be seen that Fe amount is very close to the initial values. Similar trend was observed by Kumar[64].

Photodegradation of phenolic compounds, dye and heavy metals onto TiO_2/ZrO_2 and TiO_2-Fe catalyst: The activity of TiO_2/ZrO_2 photocatalyst was tested to determine the optimal catalyst for Reactive red dye photocatalytic degradation[64]. The reaction was carried out at initial concentration of Reactive red dye 50 ppm, catalyst loading 250 mg/L and pH 7. As shown in Fig. 3, the results indicate that after 70 min, the degraded Reactive red dye is 74.79, 88.72 and 39.45 %, for different zirconia content on TiO_2 surface (ZT-2 , ZT-1, ZT-3), respectively. The degradation order of DCF of the three catalyst was ZT-2 > ZT-1 > ZT-3, which was qualitatively consistent with the order of BET surface area. With the increase of the content of Zr, decrease in the decomposition of warfare agents due to the colapse crystallinity and break down of porosity is observed. The presence of Zr^{4+} dopant therefore could suppress the growth of TiO_2 grains, increase the surface area, decrease the anatase-rutile phase transformation and accelerate the surface hydroxylation. The properties mainly, surface hydroxylation and high degradation activity of warfare agents for ZT-2 is having highest Photocatalytic activity. So, ZT-2 is the selected catalyst for further reaction.

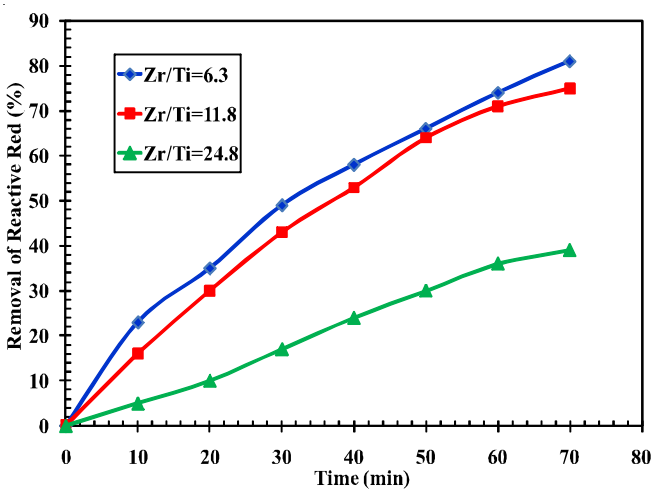

Fig. 3. Removal of reactive red in the presence of ZrO_2-TiO_2 composite with different Zr/Ti ratio [Ref. 64]

The photocatalytic activities of the ZrO_2-TiO_2 catalysts with different Zr/Ti ratio were evaluated by degradation of *p*-chlorophenol under UV light[55]. These results were compared to that of pure TiO_2 and commercially available Degussa P25. The zero minute indicates that the *p*-chlorphenol adsorption equilibrium on the catalysts at dark for 0.5 h. The ZrO_2 doped TiO_2 samples exhibit higher photocatalytic activity for degradation of *p*-chlorophenol compared to either pure TiO or P25. These results provide direct evidence that the addition of ZrO_2 -TiO_2 into TiO_2 can efficiently improve the photocatalytic activity. Liu *et al.*[55] reported that photocatalytic activity from 4 to 20 and 20 ZrO_2-TiO_2 sample shows highest photoactivity, with the degradation rate of 94.9 %. However, high Zr content (P30 %) is harmful for the activity. This may be related to its poor anatase crystallinity, decreased surface area and acidity and the poor transfer of electrons from ZrO_2 to TiO_2[65,66,55].

The photocatalytic activity of nitrogen doped ZrO_2/TiO_2 photocatalysts with different nitrogen doping contents (0.1, 0.15, 0.2 and 0.4 M) was evaluated under both UV and visible light (Figs. 4 and 5)[59]. The results clearly illustrate that the photocatalytic activity increase with an increase in nitrogen content until the optimum value of 0.15 M is reached. The maximum recorded photodegradation efficiencies for UV and visible light irradiation were 99 and 92 %, respectively. When the nitrogen doping content exceeded the optimum value, the photocatalytic activity decreased dramatically relative to the maximum, especially under visible light irradiation. This phenomenon fits well with the rule put forth by Wang *et al.*[67]

and Sreethawong *et al.*[68]. As described above, the presence of a higher amount of nitrogen was found to be detrimental to the photocatalytic activity. There are two possible reasons that may explain the decrease of photocatalytic activity at nitrogen doping contents higher than 0.15 M including the formation of TiN, which is metallic and non-transparent to visible light[69] and an increase the concentration of oxygen-vacancies, which serve as recombination centers for holes and electrons and therefore, decrease the quantum yield of the photocatalytic activity[70]. Because of the above mentioned reasons, 0.15 M was selected as the optimum nitrogen doping content. Fig. 6 shows the effect of initial NO concentration on photodegradation of NO. The efficiency of NO degradation decreases as the initial NO concentration increases from 4 to 10 ppm. Under UV light irradiation, the degradation efficiency maintained a high value (98%) at the initial NO concentration of 4 and 6 ppm (Fig. 6). The degradation efficiency (90 %) under visible light irradiation at the initial NO concentration of 4 ppm was apparently higher than the degradation efficiency (20-40 %) at initial NO concentrations of 6, 8 and 10 ppm. The decrease in photodegradation efficiency with an increase in the initial concentration of NO is typically related to three factors: Adsorption capacity, generation and transfer of photo-generated electron-hole pairs followed by reaction between an electron-hole pair and NO and the generation of intermediate product[59]. It should be noted that the effect of the intermediate product was not taken into account. Generally, the Langmuir-Hinshelwood (L-H) kinetic mechanism is widely used to describe photodegradation reactions[71-75]. All sites of photocatalysts are saturated with NO at a certain concentration, CNO, S; therefore, the NO concentration at the photocatalyst surface does not increase at initial NO concentrations higher than CNO, S. This may lead to a decrease in the resulting efficiency of NO degradation. Furthermore, at higher concentrations, the generation of electron-hole pairs, which are excited by light becomes the control step and the sensitivity of the electron-hole pairs on light dominates the rate of photo-degradation reaction. At the same intensity of light irradiation, UV light can produce more electron-hole pairs than visible light. Therefore, the degradation under UV light irradiation is better than that under visible light irradiation.

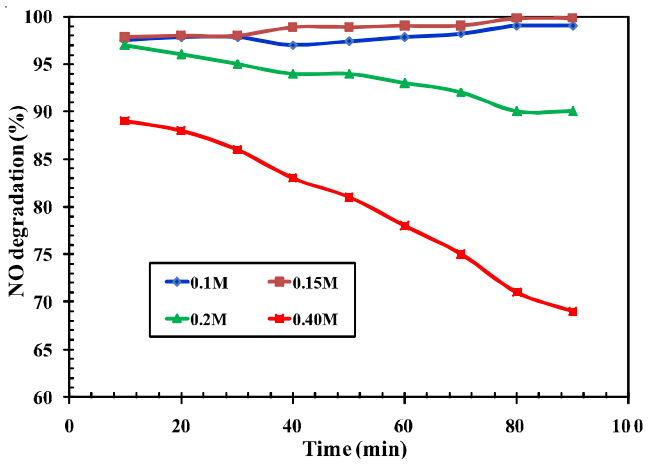

Fig. 4. Degradation of NO in the presence of UV [Ref. 59]

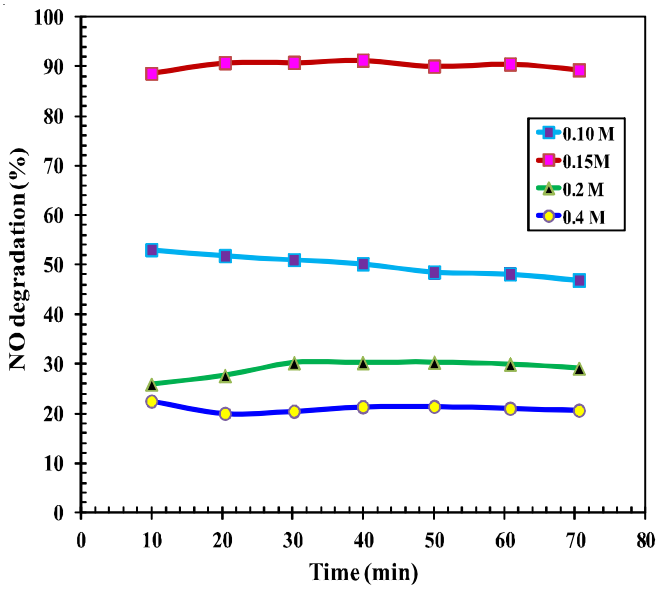

Fig. 5. Degradation of NO in the presence of visible light [Ref. 59]

The highest efficiency of photocatalytic degradation was obtained at the initial NO concentration of 6 ppm under UV and 4 ppm under visible light irradiation (Fig. 6). Light irradiation is the driving force of photocatalytic reactions and the intensity of irradiation directly influences the Photocatalytic reaction rate. As light intensity increases, more electron-hole pairs are produced. However, if the light intensity is excessive, electron-hole pairs recombine and rate of electron-hole recombination increases relative to the rate of interfacial charge transfer. In other words, excessive light intensity leads to lower quantum efficiency[72]. Yang and Lui[76] considered that increase of electron-hole recombination with the increase of light intensity might lead to an increase in the temperature of the catalysts, which results in decreased adsorption capacity (Figs. 7 and 8). Therefore, it is essential to determine the appropriate light intensities for NO degradation to effectively utilize light energy and ensure the desired degradation performance. Figs. 9 and 10 show the photodegradation of NO with varied light intensity, which was controlled by changing number of lamps from 1 to 4. It is clear that there is little difference (from 97 to 99 %) in degradation of NO.

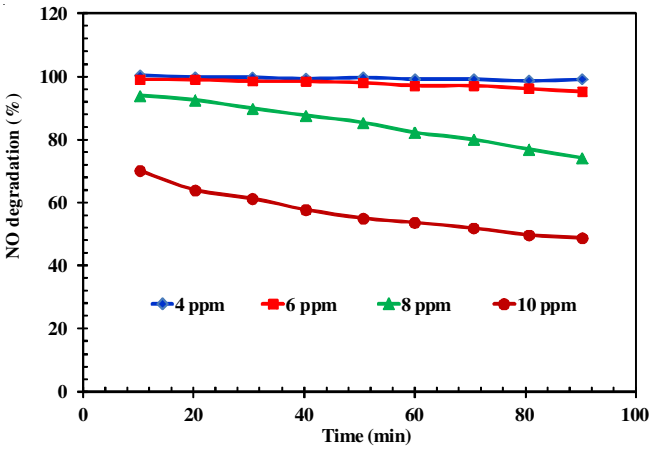

Fig. 6. Effect of concentration on degradation of NO in the presence of UV [Ref. 59]

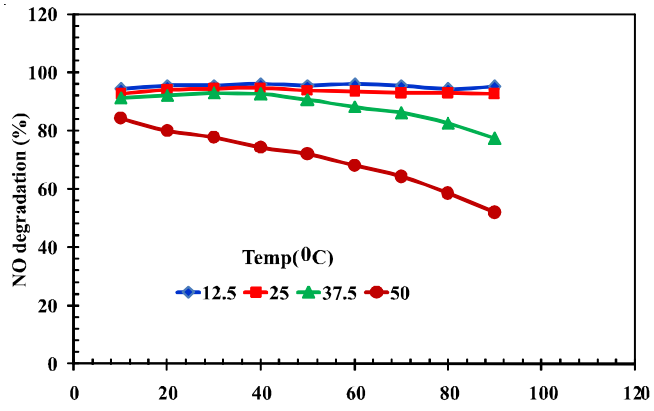

Fig.7. Degradation of NO using UV light [Ref. 59]

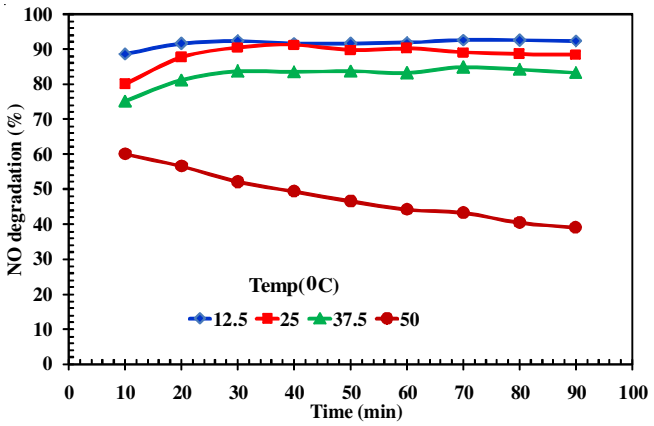

Fig. 8. Degradation of NO using visible light [Ref. 59]

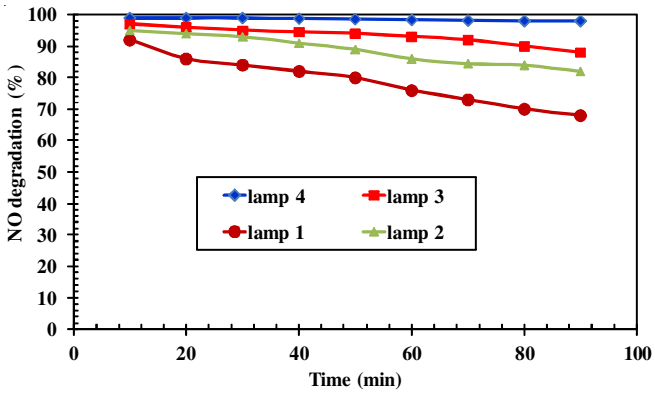

Fig. 9. Effect of lamp on degradation of NO using UV light [Ref. 59]

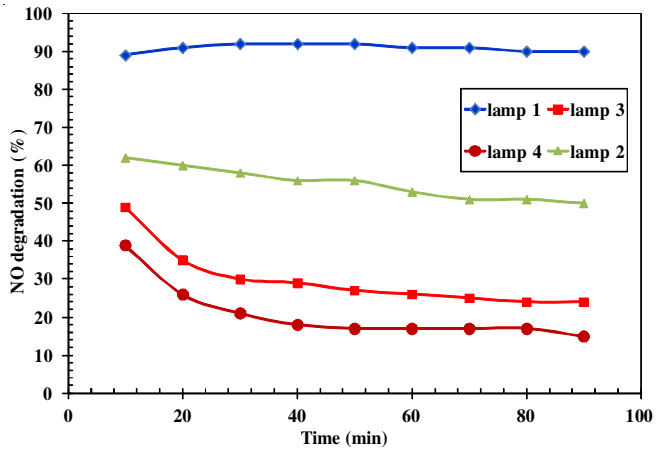

Fig. 10. Effect of lamp degradation of NO using visible light [Ref. 59]

Synthesis of the composites and constituent compounds ZrO_2 was synthesized by polyol method[58]. In brief, a mixture of aqueous solution of $ZrOCl_2 \cdot 8H_2O$ and ethylene glycol was refluxed at 100 °C for 1 h. Urea dissolved in ethylene glycol and water mixture (1:1 by volume) was added to the clear solution containing the precursor ions and refluxed at 180 °C for 4 h. The precipitate obtained was separated by centrifugation, washed and dried in an oven at 90 °C for 5 h followed by calcination in air at 500 °C for 4 h. Titanium dioxide was synthesized by the hydrolysis of titanium isopropoxide. Required amount of titanium isopropoxide in isopropyl alcohol (IPA) was taken (1:1 ratio by volume). Water was added to the mixture drop by drop under constant stirring to hydrolyze the titanium isopropoxide. The precipitate was dried in an oven at 110 °C for 5 h followed by calcination at 500 °C for 4 h in air. Titanium dioxide (30 % by weight) was dispersed on ZrO_2 (ZT, ZrO_2:TiO_2 = 1:0.46 by mole) by the hydrolysis of titanium isopropoxide on ZrO_2. Required amount of titanium isopropoxide in isopropyl alcohol was added to the support powder and water was added to the mixture under constant stirring to hydrolyze the titanium isopropoxide. The resultant mixture was evaporated to dryness followed by heating the powder at 500 °C for 4 h. Cadmium sulfide (30 % by weight) was loaded on ZrO_2 and TiO_2 (named as ZC, ZrO_2:CdS = 1:0.26 by mole and TC, TiO_2: CdS = 1:0.17 by mole, respectively) by an impregnation method. Aqueous solution of cadmium was stirred with the support powder and evaporated to dryness. The cadmium chloride adsorbed on the support was heated with an aqueous solution of thiourea. The resultant mixture was evaporated to dryness followed by heating the powder at 350 °C for 2 h. ZrO_2-TiO_2-CdS was synthesized by a multistep impregnation method. First, TiO_2 (30 % by weight) was loaded on ZrO_2 by the hydrolysis of titanium isopropoxide. The ZrO_2-TiO_2 powder was calcined in air at 500 °C for 4 h. Cadmium sulfide (30 % by weight of ZrO_2-TiO_2) was loaded on ZrO_2-TiO_2 by the impregnation method. The resultant mixture was evaporated to dryness followed by heating the powder at 350 °C for 2 h. Pure CdS was prepared by polyol method. Cadmium chloride (4 g) dissolved in water was mixed with ethylene glycol and refluxed at 100 °C for 15 min. At this stage, thiourea (2 g, thiourea/Cd = 4) dissolved in water and ethylene glycol was added to the solution and refluxed at 120 °C for 4 h. The precipitate obtained was washed with acetone and ethyl alcohol three times each and heated at 350 °C for 2 h in air. Palladium (0.5 % by weight) was loaded on ZTC (Pd-ZTC) and CdS (Pd-CdS) by a wet impregnation method. Sample powder was kept in contact with aqueous palladium chloride solution and evaporated to dryness under constant stirring followed by heating in air at 350 °C for 2 h. No reductive treatment was given to these catalysts before photocatalysis experiment. Palladium oxide particles were reduced to Pd metal during the initial hours of irradiation, which was confirmed by change in color of the suspension from orange red to gray. Palladium concentration on these catalysts was varied to obtain the optimum concentration of the metal, which can lead to relatively higher photocatalytic activity. Sasikala *et al.*[58] concluded that supports play a significant role in enhancing the photocatalytic activity of CdS. Effect of Pd cocatalyst on the photocatalytic activity of ZTC, which is the best sample

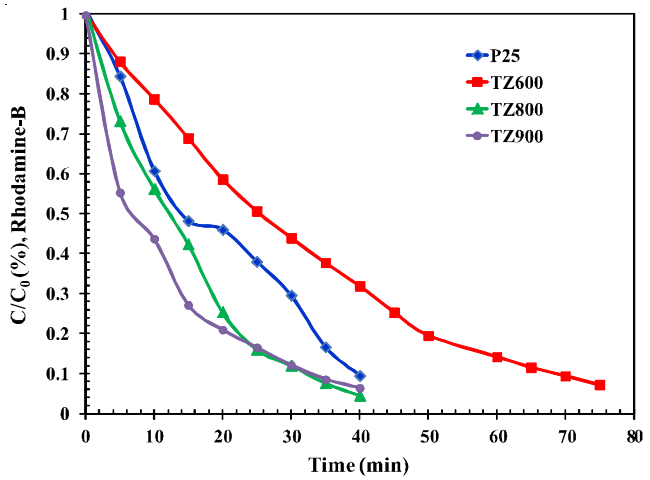

Fig. 11. Meso 50TZ calcined at different temperature on degradation of rhodamine-B (600, 800, 900 °C) [Ref. 56]

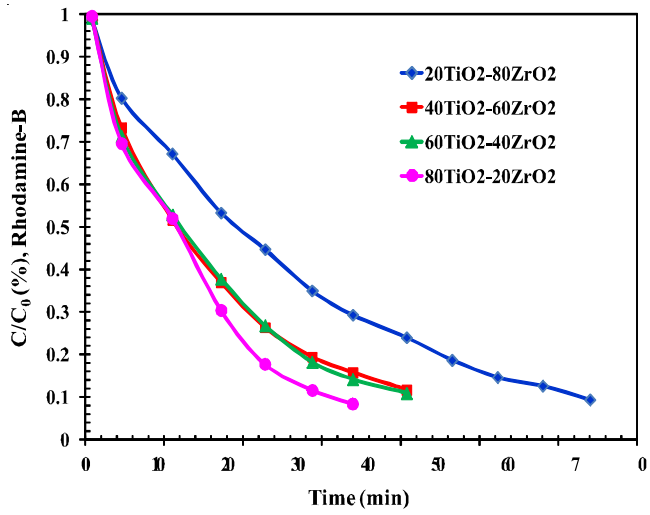

Fig. 12. Change in concentration in the presence TiO_2-ZrO_2 composite at different ratio of Ti/Zr ratio [Ref. 56]

among the composites. A very high increase in the photocatalytic activity is observed for both in the presence of Pd co-catalyst. An apparent quantum efficiency of 11.5 % is obtained for Pd/ZTC photocatalyst.

For the Rhodamine-B solution using meso-50TZ calcined at 800 °C as catalyst clearly shows the decoloration process of Rhodamine-B solutions along with irradiation time[56]. Therefore, the concentration of Rhodamine-B is evolved using the linear part of the absorbance-concentration curve (Beer's Law) and measuring absorbance out the corresponding concentration. The photocatalytic activity of commercial nonporous photocatalyst P25 was also measured under the same condition for the purpose of comparison. Fig. 11 displays the time profiles of C/C_0 under UV light irradiation for meso-50TZ calcined at different temperatures, where C is the concentration of Rhodamine-B at the irradiation time t and C_0 is the initial concentration. After light on, the concentration of Rhodamine-B decreased with irradiation time and the pseudo-first-order reaction is observed. Samples calcined at 400, 800 and 900 °C all present good catalytic efficiency and the degradation process finished within 40 min, which is comparable with the commercial P25. Fig. 12 shows the time profiles of C/C_0 under UV light irradiation for the representative samples with different Ti/Zr ratios. This order obviously indicates that the reactivity becomes higher with the increase of sample crystallinity. Furthermore, representative samples with variable Ti/Zr ratios are also tested for degradation of Rhodamine-B. The meso porous composites of 20TZ, 40TZ, 60TZ and 80TZ exhibit photocatalytic activities which are major related to the Ti/Zr ratio. It is found that decomposition rate per surface area follows the order of 80TZ > 60TZ > 40TZ > 20TZ. With an increase in the content of Ti, the degradation amount of Rhodamine-B increases. This increase in activity is reasonable when the following points are taken into consideration: first, zirconia has a large band gap, greater than 5 eV, so it cannot act as a photocatalyst under the irradiation conditions used for these experiments. Yuan *et al.*[56] found crystallinity gradually improved with the increase of Ti. Most of our meso-porous TiO_2-ZrO_2 samples show higher photocatalytic activities than P25 except TZ600. Compared to P25, the Ti ratios of our samples are lower, while the surface areas are larger. The sufficient amount of Zr inhibits remarkably crystallization and the consequent structural growth, resulting in high surface areas. Large surface areas and pore volumes are beneficial to more Rhodamine-B molecules absorbed in the channels to contact with active sites. The mesoporous TiO_2-ZrO_2 composites exhibit a binary function for the degradation of Rhodamine-B derived from their crystalline of the framework and high surface areas.

No detectable degradation of Rhodamine-B occurs without micro-arc oxidation surface under UV light radiation. It is proved that the photocatalytic decomposition of Rhodamine-B solution agrees with the apparent first-order model[77]. The photocatalytic reaction rate constants of degradation of Rhodamine-B solution with ZrO_2/TiO_2 composite and pure TiO_2 under UV irradiation are measured as 0.0442 and 0.0186/h, respectively. A comparison between the photocatalytic activities of the two surfaces emphasizes the photocatalytic enhancement in the ZrO_2/TiO_2 composite, which can be mainly attributed to the mixed phase, more surface sites and formation of structural defects. The ZrO_2/TiO_2 composite has the mixed phase of anatase, rutile and ZrO_2, which results that the photogenerated electron can transfer from rutile to anatase. This effectively inhibits the recombination of photo-generated electron-hole pairs. The lamellar and porous microstructure, agglomerated ZrO_2/TiO_2 mixed particles and micro-pores in the inner layer should be responsible for providing more surface sites, in which more absorbed organic compounds can be degraded by OH^- . Furthermore, some oxygen might be escaped from the surface of the lattice to trap the photogenerated holes because of the formation of vacancies on the surface[78]. In addition, metal oxides with more structure defects on surface are able to substantially ionosorb oxygen, in the form of O_2^- species, which are involved in electron capture in aqueous phase reactions, to let photoholes react with surface OH^- groups[79]. Another reason of the enhanced photocatalytic activity is zirconia modified titania with higher surface acidity, the surface sites with higher acidity may prove to be better adsorption sites or hole traps[80].

ZrO_2/TiO_2 composite with a lamellar and porous morphology was successfully produced in the electrolyte consisted of *in*

situ $Zr(OH)_4$ colloidal particle by the micro-arc oxidation technique[60]. The composite consists of anatase, rutile and ZrO_2 phases. The optical absorption edges of the ZrO_2/TiO_2 composite and the pure TiO_2 are about 421 and 412 nm, respectively. It is also revealed that the photocatalytic activity of ZrO_2/TiO_2 composite enhances approximate three times compared with pure TiO_2 under UV irradiation. Future works will be focused on the further improvement of photocatalytic activity of ZrO_2/TiO_2 composite under ultraviolet and visible irradiations by adjusting process parameters, such as power voltage, reaction time and electrolyte composition.

Compared to pure TiO_2, the Fe-TiO_2 catalysts exhibited a significant increase in 4-nitrophenol photodegradation efficiency[60]. Zhao *et al.*[60] observed that presence of iron species influences the photocatalytic activity. At the beginning, the photocatalytic activity of the catalysts decreased with the increase of Fe^{3+} loaded onto TiO_2, while after 45 min it increased by further increasing the Fe for the 1 % Fe-TiO_2 content, except sample. This finding can be explained by taking into account the occurrence of a high iron ions leaching into solution. All of the doped samples showed to be more photoactive than pure TiO_2 and the optimal amount of Fe^{3+} are 1 %. 67.53 % Total organic carbon of a solution containing 20 mg/L 4-nitrophenol, for instance, was removed after 60 min of irradiation by using the 1 % Fe-TiO_2 sample. The beneficial effect of the presence of Fe^{3+} species on the photocatalytic activity could be due to the role of Fe^{3+} species acting as h^+/e^- traps, thus hindering the recombination rate and enhancing the photocatalytic activity.

Consequently the presence of iron species, especially at low levels, inhibits the recombination rate of h^+/e^- pair and enhances the photocatalytic activity. When the amount of iron ions is increased, they become recombination centers resulting in lowered photocatalytic activity. It has also been proved that the excess of deposited iron on TiO_2 can form $Fe(OH)^{2+}$ species, with a greater absorption of the incident light in the range 290-400 nm with respect to pure TiO_2. This competition in photon absorption subtracts photon to TiO_2 and can be considered responsible for the decrease of the photocatalytic activity of the Fe-TiO_2 samples[81,82] are scrutinized it on the photocatalytic activity is not obvious and differences in photocatalytic activity are likely due to differences in BET-surface areas.

The specific surface areas of prepared catalyst, 51-76.3 m^2/g which is similar value of the existing literature[83] and 65.1-85.6 m^2/g[82] are much larger than that of ours (only about 8 m^2/g). Moreover other morphological and physico-chemical parameters, as for instance impurities, lattice mismatches and density of surface hydroxyl groups, can affect not only the adsorption extent of the starting molecule and/or the intermediates, but also the recombination rate and thus the lifetime of the photoproduced electron-hole pairs. Further investigation will be aimed to characterize more deeply the surface of the photocatalysts in order to obtain insights on this point. Pure TiO_2 exhibits low photocatalytic property due to rapid recombination of photo-activated electrons and holes. Fe^{3+} was considered to dope into TiO_2 photo catalyst in order to enhance the photocatalytic property. The Fe^{3+} doped TiO_2 nanoparticles were prepared by sol-gel method and calcined at 400 °C for 2 h. Photocatalytic activity was determined by means of degradation of methyl orangesolution under UV light irradiation. Fe^{3+} doping into TiO_2 has an effect on inhibition of anatase crystal growth, led to the enlargement of the composite specific surface area. Therefore, the photocatalytic activity of Fe^{3+} doped TiO_2 composite in proper concentration was greater than those of pure TiO_2 and 0.5 mol % Fe^{3+} doping exhibited the highest photocatalytic activity[61].

The transition metal ion used as dopants is able to enhance the attachments of the functionalized organic pollutants to the doping ion active sites[61,84]. Fig. 13 shows the degradation of methyl orange solution using Fe^{3+}-doped TiO_2 powders, pure TiO_2 and doped TiO_2 powders under UV light for 15 min until 90 min[61]. The degradation effect of methyl orange by Fe^{3+}-doped TiO_2 in some concentrations of Fe^{3+} was better than those of pure TiO_2[85]. After 90 min of testing, the percentage degradation was 32 (pure TiO_2), 35 (0.3 mol %), 65 (0.5 mol %), 45 (0.8 mol %) and 39 (1.0 mol %) of Fe^{3+}, respectively. This increase in photocatalytic activity with Fe doping is related to shift in optical absorption of the catalyst in visible region. Titanium dioxide absorbs only UV energy (below 400 nm) whereas Fe doped catalyst absorbs UV and portion of visible energy hence there is increase in photo-catalytic activity. The presence of metal ions on the surface of the photo catalyst particles improves the rate of electron transfer to O_2 and consequently has a beneficial effect on the photo-oxidation rate of organic species. The more number of pores increases the hydroxyl content. These surface hydroxyl radicals formed on the surface of the photo-catalyst are oxidizing species which ultimately affects the photo-catalytic activity. This suggests that the increase in hydroxyl content of the film increases the photo-catalytic activity. It is also stated that these dopant exists only as the recombination centre for the electron/holes, thus having no noticeable effect on the reaction rate.

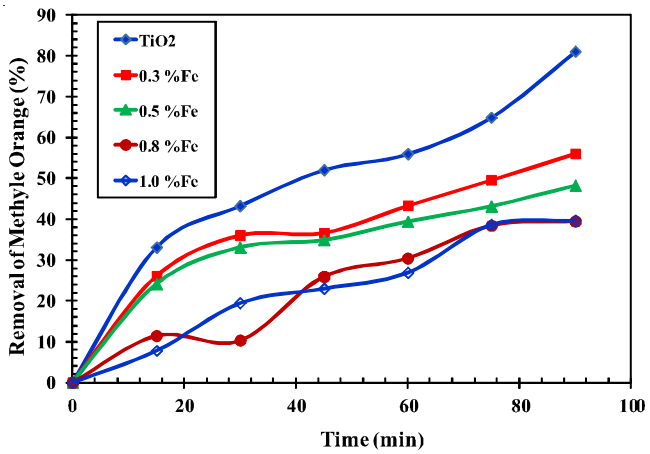

Fig. 13. Degradation of methyl orange pure and doped TiO_2 [Ref. 61]

Fig. 14 shows the dependence of $\ln(C_0/C)$ on time of the Fe-doped TiO_2 samples photodecomposing aqueous solution of methyl orange. The blank experiment shows that the methyl orange cannot be degraded in the absence of either TiO_2 or UV light. The Fe doping obviously influences the photocatalytic activity under UV light illumination. The 0.3 at. % Fe-doped sample has the best activity, better than the photocatalytic activity of P25. An optimal Fe concentration for the Fe-doped TiO_2 to present the best photocatalytic activity was

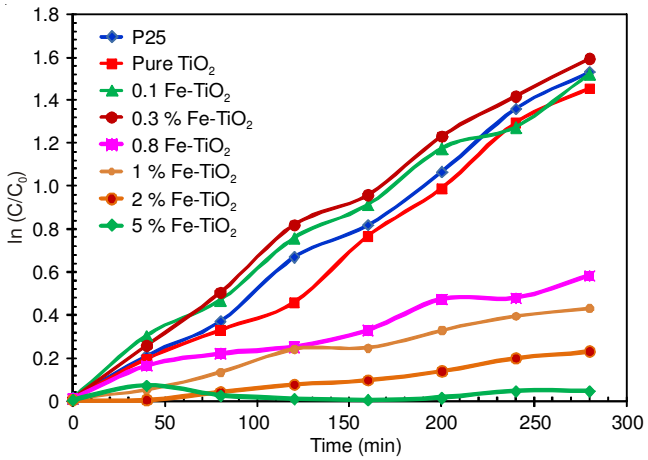

Fig. 14. Dependence of ln(C_0/C) on the UV illumination time of Fe-doped TiO_2 [Ref. 52]

observed, which is not a surprise because this has been seen for many times. Although it is stated that the Fe ions mainly form trapping centers for holes and electrons for low doping level, while they will become recombination centers for high doping[86], the mechanism of this trapping to recombination transformation is still not clear and require more study. Pathway for Fe^{4+} and Fe^{2+} ions to regenerate Fe^{3+} ions is to recombine with the holes in visible light, which are also supported by the photoluminescence spectra. Therefore, the bulk-doped Fe ions mainly from the recombination centers of electrons and holes; more Fe ions entering TiO_2 bulk cannot contribute to the photocatalysis. Compared with the Fe^{3+} ions in bulk, the Fe^{3+} ions on surface have different coordination environment. They can directly combine with the oxygen molecule (Fe-O_2) or the hydroxyl groups (Fe-OH), so the electrons or holes trapped on surface Fe^{3+} ions are possible to transfer to O_2 and -OH, resulting in the formation of O_2^- and $^{\bullet}$OH, which has also been reported by others. Therefore, the Fe ions on surface can form intermediate pathways for the interfacial transfer. Because the surface recombination of the trapped electrons and holes is generally much slower than the interfacial transfer[31], the presence of Fe^{3+} ions on surface is useful to improve photocatalytic speed. For the present experiment, the Fe^{3+} ions are not uniformly distributed in TiO_2 nanoparticles. In case of the low-level doping, they are mainly on TiO_2 surface. According to the above discussion, it can be known that the Fe ions mainly form the pathway for the electron-hole transfer for low doping concentration, so the photocatalytic activity will increase with the increase of doping concentration. For high-level doping, many Fe^{3+} ions can be doped in bulk beside those on the surface, so the recombination through the bulk Fe^{3+} ions cannot be neglected. Therefore, the photocatalytic activity firstly increases and then decreases with the increase of doped Fe content. It is widely accepted that the doped Fe^{3+} ions will change from the trapping centers to recombination centers as the doped concentration increases, how this change takes place is still not clear. It is claimed that the tunnel recombination through Fe ions is the reason of this trapping to recombination changing. Previous workers[52] had given new explanation of the trapping to recombination changing with the increase of Fe concentration, which is related to surface doping and bulk doping, as illustrated above.

The commercial photocatalyst (Degussa P25) was also used in the experiment to compare with synthesized photocatalysts. When the UV lamp was turned on (t = 0), the production rate of photo-induced electrons and holes was suddenly excited, resulting in immediate removal of 1,2-dichloroethane, although reaction rate tended to stabilize or decrease later on. The photocatalytic activity of TiO_2 tested at room temperature = 120 s is the highest (conversion, h = 98 %), followed by that tested at 60 s (h = 79 %) > Degussa P25 at 30 s (h = 59 %) > TiO_2 at 30 s (h = 49 %) at the end of experiments. It indicates that the conversion is a function of room temperature within the range from 30 s to 120 s. Water was found to play an important role in heterogeneous photocatalysis[87]. The H_2O adsorbed on the surface of TiO_2 will be oxidized by h^+ and produce OH radicals. However, more water vapor will make competitive adsorption on the active site of TiO_2 compared with pollutants[88].

The conversion for 1,2-dichloroethane for photocatalysts with Fe-doping systems all remained relatively stable. The photocatalytic activity follows the order: Fe/Ti = 0.001 mol % (h = 72 %) > Fe/Ti = 0.01 mol % (h = 62 %) > Degussa P25 (h = 58 %) > Fe/Ti = 0.05 mol % (h = 51 %) > Fe/Ti = 0 mol % (h = 48 %) at the end of experiments. Somehow, the role of Fe must play an important role during the photocatalytic reaction. It is speculated that the higher photocatalytic activity of Fe/Ti = 0.001 mol %, is due to either one or combination of the following factors: (i) increased UV light absorption capability of Fe-TiO_2 compared to synthesized raw TiO_2, P25 or other Fe-TiO_2; (ii) form a lesser rutile phase (lower photocatalytic activity) due to a small amount addition of Fe^{3+} compared to other Fe-TiO_2; (iii) alleviate the surface poison phenomenon; and (iv) act as both h^+/e^- traps to reduce the recombination rate of h^+/e^- pairs during the photodegradation. When iron ions doping concentration is increased, the ions become recombination centers resulting in reduced photocatalytic activity[89]. Since the photocatalytic reaction occurs on the surface of TiO_2, surface area plays another important role in the photocatalytic reaction. However, the addition of Fe^{3+} decreases the surface area of Fe/TiO_2 (Table-1), therefore, the surface area alone cannot be used to explain the observed phenomena. The role of Fe mentioned above may be responsible for the enhanced photodegradation of 1,2-dichloroethane, as compared to those from P25 or synthesized nude TiO_2.

Literature remarks and future suggestions: The introduction of ZrO_2 not only retard the phase transformation from the anatase phase to the rutile phase, but also inhibit the crystallite growth and aggregation, which resulted in the resultant mesoporous ZrO_2-TiO_2 materials possessing high specific surface areas and thermal stability[55]. Furthermore, compared with pure TiO_2 obtained mesoporous ZrO_2-TiO_2 composites exhibit stronger absorption in ultraviolet region and increased surface acidity in the form of OH groups. The ZrO_2-TiO_2 samples exhibit high photocatalytic activity under UV for the degradation of *p*-chlorophenol. Visible-light responsive nitrogen doped ZrO_2/TiO_2 photocatalysts were synthesized *via* a sol-gel process[59].

Cha *et al.*[59] suggested that nitrogen was doped in the lattice of TiO_2 and had an effect on the translation of phase, photodegradation activity and visible-light response. Among synthesized photocatalysts, 0.1 M Zr and 0.15 M nitrogen supported

on TiO_2 exhibited the best visible-light response and the highest NO photodegradation activity. A series of visible-light responding nitrogen doped ZrO_2/TiO_2 photocatalysts were synthesized, characterized and used to degrade NO under both UV and visible light irradiation[59]. The characterization results demonstrated that the addition of nitrogen was favored to the anatase-rutile phase transformation and visible-light reactivity. It was also noted that the average diameter of the photocatalyst particles increased with an increase in the nitrogen doping content. Under visible light irradiation, the nitrogen doping content had a considerable effect on photocatalytic activity and the initial NO concentration and light intensity were the limiting factors. A hybrid photocatalyst of ZrO_2-TiO_2-CdS shows enhanced photocatalytic activity for hydrogen generation from water as compared to its constituent single phase oxides, TiO_2-CdS and ZrO_2-CdS[62]. In this nano-composite photocatalyst, CdS exists as a dispersed phase. The lifetime of the photogenerated charge carriers is the highest in the

TABLE-1
ZrO_2–TiO_2 AND Fe-TiO_2 PHOTO CATALYSTS WITH THEIR PARAMETERS AND ITS APPLICATIONS

S. No.	ZrO_2–TiO_2/Fe- TiO_2 Photocatalyst	Pollutant (s)	Remarks	Reference
1.	TiO_2 samples impregnated with functionalized Cu(II)- or metal-free porphyrins	4-Nitrophenol	Rate of electron transfer to this very oxidant adsorbed species (in addition or alternative to $3O_2$) from the conduction band of TiO_2 and/or from Cu(I) species possibly produced under irradiation is hypothesized to be mainly responsible for the enhancement of the reaction rate of the global Photocatalytic process.	90
2.	Sol–gel preparation of TiO_2–ZrO_2 thin films supported on glass rings	Photocatalytic removal of VOCs, acidic sols of different composition (ZrO_2, TiO_2 and Ti–Zr mixed oxides)	Same Zr content, the photoactivity of the films containing binary metal oxides is slightly higher than that of the solid solution	25
3.	Commercial TiO_2 powders	Phenol and *m*-nitrophenol	Optimal solution pH for photodegradation of phenol and *m*-nitrophenol could be realized and obtained at 7.4 and 8.9, respectively	91
4.	Carbon nanotube/TiO_2 Composite	Methylene blue	Carbon Nanotube/TiO_2 particle with UV and electro-chemical reaction appeared an excellent degradation effect with reaction time, due to the increase of electrical conductivity and electro-oxidation activity	92
5.	Titania-zirconia composites	Rhodamine-B	Nanocomposites with controlled texture properties composition are obtained in a wide range from 10 to 90 mol% TiO_2	56
6.	Fe_2O_3-TiO_2 coatings were prepared on glass slide substrates using sol-gel method	Rhodamine-6G	15 wt % Fe_2O_3 modified TiO_2 film is the optimal photocatalyst to degradation	93
7.	Fe-doped titanium dioxide (Fe-TiO_2)	Phenol	Visible light irradiation from sun, UV light sources with 190 and 390 nm, fluorescence and dark environment were used and found that the degradation of phenol was in the order of 7.8%, 12%, 7.5%, 6.8% and 5% obtained after 24 h, respectively.	94
8.	Fe–TiO_2 heterogeneous	4-Nitrophenol	Removal of 67.53% Total organic carbon at C_0 = 20mg/l (4NP), 60 min reaction time.	60
9.	TiO_2/kaolinite (TiO_2/Kao)	Acid red G and 4-nitrophenol	After 90 min of Irradiation, the degradation of Acid red G was nearly100%.	57
10.	TiO_2 doped with selective transition metals	Azo dyes	Transition metal doped TiO_2 has been found to be very effective for the remedial of azo dye-contaminated solutions.	95
11.	Mono-functionalized porphyrin derivative, 5-mono-[4-(2-(4-hydroxy)-phenoxy)ethoxy]-10,15,20-triphenylporphyrin (3) and its Cu(II) (3a), Zn(II) (3b) and Ni(II) (3c) metalloporphyrins	4-Nitrophenol	all the 3a, 3b, 3c enhanced the photocatalytic efficiency of bare TiO_2 in photodegrading the 4-NP, and 3a-TiO_2 exhibited the highest photocatalytic activity	96
11.	TiO_2 doped with transition metal ions like V^{5+}, Mn^{2+}, Fe^{3+}, Ru^{3+}, Os^{3+}, Ni^{2+} and Zn^{2+}	Indigo Carmine and 4-nitrophenol	Irrespective of excitation source UV/solar light and nature of the organic pollutant, photocatalytic activities of doped photocatalysts followed the order: Mn^{2+}-TiO_2 >Fe^{3+}-TiO_2 >Ru^{3+}-TiO_2 ≥ Os^{3+}-TiO_2 >Zn^{2+}-TiO_2 >V^{5+}-TiO_2 >Ni^{2+}-TiO_2 at an optimum concentration of dopant	97
12.	ZrO_2/TiO_2 photocatalysts *via* a sol–gel process	Nitric oxide (NO)	0.1 M Zr and 0.15 M N supported on TiO_2 exhibited the best visible-light response and the highest NO photodegradation activity	59
13.	ZrO_2–CeO_2–TiO_2 visible light photocatalyst	Rhodamine B	90 % removal of Rhodamine B after 160 min irradiation in the ZrO_2–CeO_2–TiO_2 composite	42

14.	TiO_2 and sulfate modified	Acetaldehyde	Modifications of the acid–base properties of TiO_2-based photocatalysts can be used to improve their sustained activity.	98
15.	Mesoporous ZrO_2–TiO_2 nanocomposites		The photocatalytic activity of the ZrO_2–TiO_2 sample is higher than that of the TiO_2 sample and commercially available Degussa P25.	55
16.	ZrO_2–TiO_2–CdS composite	Hydrogen generation	Hybrid catalyst exhibits increased Photocatalytic activity for hydrogen generation from water as compared to their constituent compounds	58
17.	TiO_2–Fe_2O_3 powder with and without Na_2SiO_3 additive	Acetone, nitric oxide	UV Photo activity was higher for acetone than gaseous nitric oxide.	99
18.	ZrO_2/TiO_2 composite photocatalytic film by micro-arc oxidation	Rhodamine B	the photocatalytic reaction rate constants of degradation of rhodamine B solution with ZrO_2/TiO_2 composite film and pure TiO_2 film under ultraviolet irradiation are measured as 0.0442 and 0.0186/ h respectively	26
19.	Eosin Y-sensitized mesoporous-assembled TiO_2–ZrO_2 mixed oxide nano crystal photocatalysts	Hydrogen production by photocatalytic water splitting	hydrogenproductionrevealedthattheTiO2–ZrO_2 mixedoxidephotocatalyst,withaTiO2- to-ZrO_2 molar ratio of 95:5,calcined at 800 ^{0}C for 4h, provided maximum photocatalytic hydrogen production activity	100
20.	Fluorescein, Rhodamine B, and Chlorophyll-Cu supported on ZrO_2	Photochemical water splitting performance	The highest efficiency of hydrogen generation under air mass 1.5 global (AM 1.5 G) illumination (solar simulator) was 0.058 ml/cm2-h when a ZrO_2 nanoparticles layer was coated with sodium copper chlorophyll and rhodamine B	101
21.	TiO_2 doped with Fe and Co by the sol-gel method	-	The type of dopant and doping method has a significant influence on the surface activity of the systems obtained by sol-gel method. Iron and cobalt were found to be effectively doped on the surface of synthetic the TiO_2 sample. EDS analysis of Fe and Co doped TiO_2 confirmed the presence of Fe and Co ions in the powder structure	63

hybrid catalyst. The increased activity of the multicomponent catalyst is attributed to the enhanced charge transfer efficiency from CdS to ZrO_2 and TiO_2. Palladium co-catalyst enhances the activity of the hybrid photocatalyst by increasing the lifetime of the photogenerated charge carriers further and providing active sites for hydrogen evolution.

The photocatalytic activity first increases and then decreases as the Fe concentration increases, which is co-affected by the bulk-doped and surface-doped Fe ions[62]. Wen *et al.*[62] discussed different functions of Fe ions on surface and in bulk during photocatalysis under UV light illumination. It is found that the surface doping is dominant for low-level doping and more Fe ions will enter TiO_2 bulk with the increase of doping concentration. They also suggested that the role change of Fe ions from trapping to recombination centers as the doped Fe concentration increases is related to the transformation from surface to bulk doping and this transformation explains the photocatalytic behavior of Fe-doped TiO_2 observed by us and other researchers.

The photocatalyst 1 % Fe-TiO_2 was found to be more efficient than bare TiO_2[60]. Catalyst and H_2O_2 concentration, initial pH of 4-nitrophenol solution are important variables on the process efficiency. The optimum concentrations of catalyst and H_2O_2 for enhanced efficiency are 0.1 g/L and 4.9 mM, respectively. The degradation of 4-nitrophenol by the UV/Fe-TiO_2/H_2O_2 process is more favorable in acidic than in alkaline pH. Under these optimum conditions, this process can be effectively applied for the treatment of wastewater containing 4-nitrophenol. It is also observed that catalytic behavior could be reproduced in consecutive experiments without a considerable drop in the process efficiency. Moreover, the releasing of Fe^{3+} in solution was demonstrated be negligible occurring the heterogeneous photo Fenton process.

According to the results presented by Siwinska-Stefanska *et al.*[63] systems obtained after doping of selected dopants (Fe) on titania were characterized by particles of smaller diameter and lower homogeneity compare to pure TiO_2. The XRD patterns show that the addition of iron or cobalt to the titania preparation process has a significant effect on crystalline structure formation. The XRD patterns of Fe doped TiO_2 samples almost coincide with that of pure TiO_2, showing no diffraction peaks related with iron and cobalt. The type of dopant and doping method has a significant influence on the surface activity of the systems obtained by sol-gel method. The porous structure of the doped titania decreased proportionally with increasing concentration of the dopant. Surface area measurements were carried out on TiO_2 samples doped with Fe indicating that the adopted doping procedure brought some surface area change with respect to the pristine oxide. It was apparent that Fe^{3+} doping has an effect on hindrance of anatase crystal growth; therefore the crystallite sizes of TiO_2/0.5 Fe^{3+} nanoparticles 7.88 nm are smaller than those of pure TiO_2 9.166 nm. This leads to enhancement of photocatalytic activity and disinfection efficiency due to their large surface area[61]. The surface hydroxyl content increases the photocatalytic activity of the photo-catalyst[63]. TiO_2/0.5 Fe^{3+} nano materials have strong antimicrobial properties through a mechanism including photocatalytic production of reactive oxygen species that damage cell components and viruses, its potential to be activated by visible light or sunlight. Therefore these composite

TiO_2 nanoparticles will be utilized for fresh food packaging films[103]. It is confirmed from[62] results that Fe^{3+} ions are mainly doped on TiO_2 surface for low doping concentration and some Fe ions will enter TiO_2 bulk for high doping concentration. The Fe^{3+} ions on surface can form bridges for the transfer of electrons and holes, so surface doping is beneficial to the photocatalysis. It is observed that the photocatalytic activity of as-prepared Fe-doped TiO_2 firstly increases and then decreases with the increase of doping concentration, which is due to the trapping to recombination changing of doped Fe^{3+} ions. It is confirmed that this changing is related to the increase of bulk doping as the doped concentration increases.

ACKNOWLEDGEMENTS

This study was financially supported by MPCST Bhopal for R & D Project. We also thankful to MHRD and MANIT for providing facilities for experiment work.

REFERENCES

1. D. Bahnemann, *Sol. Energy*, **77**, 445 (2004).
2. S. Suresh, V.C. Srivastava and I.M. Mishra, *Theoretical Foundations of Chem. Eng*., **47**, 284 (2012).
3. P. Rajesh, B. Prasad and S. Suresh, *Int. J. Biol. Sci. Eng.*, **3**, 223 (2012).
4. D. Ramesh Raja and S. Suresh, *Int. J. Environ. Res*., **5**, 349 (2011).
5. S. Kamsonlian, S. Suresh, C.B. Majumder and S. Chand, *Asian J. Chem*., **25**, 2409 (2013).
6. M.S. Dieckmann and K.A. Gray, *Water Res*., **30**, 1169 (1996).
7. S. Suresh, V.C. Srivastava and I.M. Mishra, *Chem. Eng. J*., **171**, 997 (2011a).
8. N. Takahashi, T. Nakai, Y. Satoh and Y. Katoh, *Water Res*., **28**, 1563 (1994).
9. H. Seshadri, S. Chitra, K. Paramasivan and P.K. Sinha, *Desalination*, **232**, 139 (2008).
10. K.R. Gota, Shakti Sanago and S. Suresh, *Int. J. Curr. Eng. Technol*., **4**, 156 (2014).
11. A. Dobosz and A. Sobczynski, *Water Res*., **37**, 1489 (2003).
12. B. Tryba, A.W. Morawski, M. Inagaki and M. Toyoda, *Appl. Catal. B*, **63**, 215 (2006).
13. N. Sobana, K. Selvam and M. Swaminathan, *Sep. Purif. Technol*., **62**, 648 (2008).
14. J.F. Zhu, W. Zheng, B. He, J.L. Zhang and M. Anpo, *J. Mol. Catal. Chem*., **216**, 35 (2004).
15. Y.E. Benkli, M.F. Can, M. Turan and M.S. Celik, *Water Res*., **39**, 487 (2005).
16. N. Daneshvar, H. Ashassi Sorkhabi and M.B. Kasiri, *J. Hazard. Mater*., **112**, 55 (2004).
17. S.M. Rodríguez, J. Blanco Gálvez and C.A. Estrada Gasca, *Sol. Energy*, **77**, 443 (2004).
18. R. Andreozzi, V. Caprio, A. Insola and R. Marotta, *Catal. Today*, **53**, 51 (1999).
19. J.M. Herrmann, *Catal. Today*, **53**, 115 (1999).
20. L. Lihong, S. Dejiu, Z. Jingwu, S. Jian and L. Liang, *Appl. Surf. Sci*., **257**, 4144 (2011).
21. P. Wang, J. Li, Y. Guo and Z. Yang, *J. Rare Earths*, **28**, 798 (2010).
22. M.S. Kim, J.J. Ryu and Y.M. Sung, *Electrochem. Commun*., **9**, 1886 (2007).
23. C. Mcmanamon, J.D. Holmes and M.A. Morris, *J. Hazard. Mater*., **193**, 120 (2011).
24. M. Hirano, C. Nakahara, K. Ota, O. Tanaike and M. Inagaki, *J. Solid State Chem*., **170**, 39 (2003).
25. M.D. Hernandez-Alonso, I. Tejedor-Tejedor, J.M. Coronado, J. Soria and M.A. Anderson, *Thin Solid Films*, **502**, 125 (2006).
26. Q. Luo, Q. Cai, X. Li, Z. Pan, Y. Li, X. Chen and Q. Yan, *Trans. Nonferrous Met. Soc. China*, **23**, 2945 (2013).
27. M. Zorn, D.T. Tompkins, W.A. Zeltner and M.A. Anderson, *Environ. Sci. Technol*., **34**, 5206 (2000).
28. S.W. Liu, Z.L. Xiu, J. Pan, X.P. Cui, W.N. Yu and J.X. Yu, *J. Alloys Comp*., **437**, L1 (2007).
29. R.A. Lucky and P.A. Charpentier, *Adv. Mater*., **20**, 1755 (2008).
30. J.H. Schattka, D.G. Shchukin, J.G. Jia, M. Antonietti and R.A. Caruso, *Chem. Mater*., **14**, 5103 (2002).
31. B. Liu, K. Nakata, X. Zhao, T. Ochiai, T. Murakami and A. Fujishima, *J. Phys. Chem*., **115**, 16037 (2011).
32. W. Zhou, K.S. Liu, H.G. Fu, K. Pan, L.L. Zhang, L. Wang and C.C. Sun, *Nanotechnology*, **19**, 035610 (2008).
33. J. Zhu, J. Ren, Y. Huo, Z. Bian and H. Li, *J. Phys. Chem. C*, **111**, 18965 (2007).
34. M. Xing, J. Zhang and F. Chen, *J. Phys. Chem. C*, **113**, 12848 (2009).
35. H. Yu, H. Irie, Y. Shimodaira, Y. Hosogi, Y. Kuroda, M. Miyauchi and K. Hashimoto, *J. Phys. Chem. C*, **114**, 16481 (2010).
36. Y. Shu, H. Sun, X. Quan and S. Chen, *J. Phys. Chem. C*, **116**, 25319 (2012).
37. H.F. Ji, The Research of Diluted Magnetic Semiconductor of Co-doped ZnO Synthesized by Sol-Gel, Xi Bei University, Microelectronics Technology (2008).
38. J. Choi, H. Park and M.R. Hoffmann, *J. Phys. Chem. C*, **114**, 783 (2010).
39. S. Wang, J.S. Lian, W.T. Zheng and Q. Jiang, *Appl. Surf. Sci*., **263**, 260 (2012).
40. X. Feng, J. Zhai and L. Jiang, *Angew. Chem. Int. Ed.*, **44**, 5115 (2005).
41. Y.C. Wu, Y. Wan and J.W. Cui, *Chinese J. Nonferrous Metals*, 2430 (2011).
42. L. Mingqin, *Res. Mater. Sci*., **2**, 28 (2013).
43. A. Fujishima and X. Zhang, *C. R. Chim*., **9**, 750 (2006).
44. M. Anpo, *Pure Appl. Chem*., **72**, 1787 (2000).
45. A. Fuerte, M.D. Hernández-Alonso, A.J. Maira, A. Martínez-Arias, M. Fernández-García, J.C. Conesa and J. Soria, *Chem. Commun.*, **24**, 2718 (2001).
46. H. Yamashita, M. Harada, J. Misaka, M. Takeuchi, K. Ikeue and M. Anpo, *Photobiol. A*, **148**, 257 (2002).
47. K. Takeuchi, I. Nakamura, O. Matsumoto, S. Sugihara, M. Ando and T. Ihara, *Chem. Lett*., **29**, 1354 (2000).
48. T. Ohno, T. Mitsui and M. Matsumura, *Chem. Lett*., **32**, 364 (2003).
49. J. Yu, Q. Xiang and M. Zhou, *Appl. Catal. B*, **90**, 595 (2009).
50. Y. Liu, X. Chen, J. Li, C. Burda, *Chemosphere*, **61**, 11 (2005).
51. T. Hirai, K. Suzuki and I. Komasawa, *J. Colloid Interf. Sci*., **244**, 262 (2001).
52. D. Chatterjee and A. Mahata, *Appl. Catal. B*, **33**, 119 (2001).
53. M.H. Zhou, J.G. Yu and B. Cheng, *J. Hazard. Mater*., **137**, 1838 (2006).
54. J. Wang, T. Ma, G. Zhang, Z. Zhang, X. Zhang, Y. Jiang, G. Zhao and P. Zhang, *Catal. Commun*., **8**, 607 (2007).
55. H. Liu, Y. Su, H. Hu, W. Cao and Z. Chen, *Adv. Powder Technol*., **24**, 683 (2013).
56. Q. Yuan, Y. Liu, L.-L. Li, Z.-X. Li, C.-J. Fang, W.-T. Duan, X.-G. Li and C.-H. Yan, *Micropor. Mesopor. Mater*., **124**, 169 (2009).
57. Y. Zhang, H. Gan and G. Zhang, *Chem. Eng. J*., **172**, 936 (2011).
58. R. Sasikala, A.R. Shirole and S.R. Bharadwaj, *J. Colloid Interface Sci*., **409**, 135 (2013).
59. J.-A. Cha, S.-H. An, H.-D. Jang, C.-S. Kim, D.-K. Song and T.-O. Kim, *Advanced Powder Technol*., **23**, 717 (2012).
60. B. Zhao, G. Mele, I. Pio, J. Li, L. Palmisano and G. Vasapollo, *J. Hazard. Mater*., **176**, 569 (2010).
61. P. Kokila, V. Senthilkumar and K. Prem, *Archives of Physics Research*, **2**, 246 (2011).
62. L. Wen, B. Liu and X. Zhao, *Int. J. Photoenergy*, **10**, (2012).
63. K. Siwinska-Stefanska, D. Paukszta, A. Piasecki and T. Jesionowski, *Physicochem. Physicochem. Probl. Miner. Process*., **50**, 265 (2014).
64. M. Arun Kumar, M. Tech. Thesis, Indian Institute of Technology, Kharagpur, India (2013).
65. J.Y. Kim, C.S. Kim, H.K. Chang and T.O. Kim, *Adv. Powder Technol*, **21**, 141 (2010).
66. B. Neppolian, Q. Wang, H. Yamashita and H. Choi, *Appl. Catal. A*, **333**, 264 (2007).
67. C.Y. Wang, C. Bottcher, D.W. Bahnemann and J.K. Dohrmann, *J. Mater. Chem*., **13**, 2322 (2003).
68. T. Sreethawong, S. Laehsalee and S. Chavadej, *Int. J. Hydrogen Energy*, **33**, 5947 (2008).
69. Z. Lin, A. Orlov, R.M. Lambert and M.C. Payne, *J. Phys. Chem. B*, **109**, 20948 (2005).
70. H. Irie, Y. Watanabe and K. Hashimoto, *J. Phys. Chem. B*, **107**, 5483 (2003).
71. A. Fernández, G. Lassaletta, V.M. Jiménez, A. Justo, A.R. González-Elipe, J.-M. Herrmann, H. Tahiri and Y. Ait-Ichou, *Appl. Catal. B*, **7**, 49 (1995).

72. N.J. Peill and M.R. Hoffmann, *Environ. Sci. Technol*., **32**, 398 (1998).
73. J.-F. Wu, C.-H. Hung and C.-S. Yuan, *J. Photochem. Photobiol. Chem*., **170**, 299 (2005).
74. J. Saien and S. Khezrianjoo, *J. Hazard. Mater*., **157**, 269 (2008).
75. Q.J. Geng, X.K. Wang and S.F. Tang, *Biomed. Environ. Sci*., **21**, 118 (2008).
76. L. Yang and Z. Liu, *Energy Convers. Manage*., **48**, 882 (2007).
77. G. Liu, X. Zhang, Y. Xu, X. Niu, L. Zheng and X. Ding, *Chemosphere*, **55**, 1287 (2004).
78. J.C. Yu, J. Lin and R.W.M. Kwok, *J. Phys. Chem. B*, **102**, 5094 (1998).
79. A. Sclafani and J.M. Herrmann, *J. Phys. Chem*., **100**, 13655 (1996).
80. B. Wu, R. Yuan and X. Fu, *J. Solid State Chem*., **182**, 560 (2009).
81. X.H. Qi, Z.H. Wang, Y.Y. Zhuang, Y. Yu and J.L. Li, *J. Hazard. Mater*., **118**, 219 (2005).
82. J.C. Yu, J. Lin and R.W.M. Kwok, *J. Phys. Chem. B*, **102**, 5094 (1998).
83. Z. Ambrus, N. Balazs, T. Alapi, G. Wittmann, P. Sipos, A. Dombi and K. Mogyorosi, *Appl. Catal. B*, **81**, 27 (2008).
84. A. Di Paola, G. Marcì, L. Palmisano, M. Schiavello, K. Uosaki, S. Ikeda and B. Ohtani, *J. Phys. Chem. B*, **106**, 637 (2000).
85. R.S. Sonawane, B.B. Kale and M.K. Dongare, *Mater. Chem. Phys*., **85**, 52 (2004).
86. M. Gratzel, Heterogeneous Photochemical Electron Transfer Reactions, CRC Press, Boca Raton, Fl, USA (1987).
87. M.R. Hoffmann, S.T. Martin, W. Choi and D.W. Bahnemann, *Chem. Rev*., **95**, 69 (1995).
88. C.H. Hung and B.J. Marinas, *Environ. Sci. Technol*., **31**, 1440 (1997).
89. W.-C. Hung, Y.-C. Chen, H. Chu and T.-K. Tseng, *Appl. Surf. Sci*., **255**, 2205 (2008).
90. G. Mele, R. Del Sole, G. Vasapollo, E. García-Lopez, L. Palmisano and M. Schiavello, *J. Catal*., **217**, 334 (2003).
91. C.-H. Chiou, C.-Y. Wu and R.-S. Juang, *Sep. Purif. Technol*., **62**, 559 (2008).
92. F.J. Zhang, M.L. Chen and W.C. Oh, *Asian J. Chem*., **21**, 7077 (2009).
93. F. Chuan, T. Li, J. Qi, J. Pan and C. Cheng, *Asian J. Chem*., **21**, 2911 (2009).
94. R.A. Shawabkeh, O.A. Khashman and G.I. Bisharat, *Int. J. Chem.*, **2**, 10 (2010).
95. M.A. Rauf, M.A. Meetani and S. Hisaindee, *Desalination*, **276**, 13 (2011).
96. W.- Sun, J. Li, G.- Yao, F.- Zhang and J.-L. Wang, *Appl. Surf. Sci*., **258**, 940 (2011).
97. L.G. Devi and S.G. Kumar, *Appl. Surf. Sci*., **2779**, 257 (2011).
98. Z. Topalian, B.I. Stefanov, C.G. Granqvist and L. Österlund, *J. Catal*., **307**, 265 (2013).
99. P. Ctibor, V. Stengl and Z. Pala, *Am. Chem. Sci. J*., **3**, 387 (2013).
100. L. Kokporka, S. Onsuratoom, T. Puangpetch and S. Chavadej, *Mater. Sci. Semicond. Process*., **16**, 667 (2013).
101. Y.-S. Lai, Y.H. Su and M.I. Lin, *Dyes Pigments*, **103**, 76 (2014).
102. A. Erkan, U. Bakir and G. Karakas, *J. Photochem. Photobiol. Chem*., **184**, 313 (2006).
103. Q. Li, S. Mahendra, D.Y. Lyon, L. Brunet, M.V. Liga, D. Li and P.J.J. Alvarez, *Water Res.,* **42**, 4591 (2008).